Published in final edited form as:
J Inorg Biochem. 2013 August ; 125: 40–49. doi:10.1016/j.jinorgbio.2013.04.002.

Metal toxicity and opportunistic binding of Pb^{2+} in proteins

Michael Kirberger[1,2], **Hing C. Wong**[1], **Jie Jiang**[1], and **Jenny J Yang**[1,*]

[1]Department of Chemistry, Center for Diagnostics and Therapeutics and Drug Design and Biotechnology, Georgia State University, Atlanta, GA, 30303

[2]Department of Natural Sciences, Clayton State University, Morrow, GA, 30260

Abstract

Lead toxicity is associated with various human diseases. While Ca^{2+} binding proteins such as calmodulin (CaM) are often reported to be molecular targets for Pb^{2+}-binding and lead toxicity, the effect of Pb^{2+} on the Ca^{2+}/CaM regulated biological activities cannot be described by the primary mechanism of ionic displacement (e.g., ionic mimicry). The focus of this study was to investigate the mechanism of lead toxicity through binding differences between Ca^{2+} and Pb^{2+} for CaM, an essential intracellular trigger protein with two EF-Hand Ca^{2+}-binding sites in each of its two domains that regulates many molecular targets via Ca^{2+}-induced conformational change. Fluorescence changes in phenylalanine indicated that Pb^{2+} binds with 8-fold higher affinity than Ca^{2+} in the N-terminal domain. Additionally, NMR chemical shift changes and an unusual biphasic response observed in tyrosine fluorescence associated with C-terminal domain sites EF-III and EF-IV suggest a single higher affinity Pb^{2+}-binding site with a 3-fold higher affinity than Ca^{2+}, coupled with a second site exhibiting affinity nearly equivalent to that of the N-terminal domain sites. Our results further indicate that Pb^{2+} displaces Ca^{2+} only in the N-terminal domain, with minimal perturbation of the C-terminal domain, however significant structural/dynamic changes are observed in the trans-domain linker region which appear to be due to Pb^{2+}-binding outside of the known calcium-binding sites. These data suggest that opportunistic Pb^{2+}-binding in Ca^{2+}/CaM has a profound impact on the conformation and dynamics of the essential molecular recognition sites of the central helix, and provides insight into the molecular toxicity of non-essential metal ions.

Keywords

Calcium; calmodulin; lead; toxicity; opportunistic binding

1 Introduction

Lead toxicity is a persistent global health problem. General physiological and biochemical problems associated with lead toxicity include neurological disorders related to the central and peripheral nervous systems [1–3], interference with heme biosynthesis [4], anemia [5], nephrotoxicity [6], hypertension [7] and reproductive disorders [8–10]. Potential carcinogenic and genetic effects related to lead toxicity have been reviewed [11].

*Corresponding author: Jenny J. Yang, jenny@gsu.edu, Tel: 404-413-5520, Fax: 404-413-5551.

Ionic displacement (e.g., ionic mimicry [12]) is believed to be the primary mechanism associated with several types of Pb^{2+}-induced anemia, first identified almost a century ago [5]. Pb^{2+} has been found to displace Mg^{2+} in pyrimidine 5'-nucleotidase type 1 [13], inhibiting the activity of the enzyme. This decreased activity results in increased concentrations of pyrimidines with an increased rate of destruction of red blood cells leading to anemia [14]. Pb^{2+} has also been shown to replace Zn^{2+} in 5-aminolevulinic acid dehydratase (ALAD) [15, 16], an important enzyme in heme synthesis, resulting in iron-deficiency anemia. Iron is another important metal which may be a target for Pb^{2+} displacement. Iron plays important roles in heme biosynthesis, including the formation of the heme precursor protoporphyrin, and in the function of ribonucleotide reductase (RNR) which catalyzes the formation of deoxyribonucleotides through a free radical mechanism. The extent to which Pb^{2+} may be able to directly interfere with the biological roles of iron is not known, but Pb^{2+} has been found to displace Fe^{2+} in divalent cation transporter-1 [17] which may be involved in transport of Pb^{2+} and cellular uptake, and in the crystal structure of RNR.

Ca^{2+} binding proteins have also been identified as molecular targets for Pb^{2+} binding and lead toxicity. Pb^{2+} can enter cells through Ca^{2+} channels [18, 19], and can displace Ca^{2+} in different Ca^{2+}-binding proteins (CaBPs) [20–24]. Protein kinase C (PKC), a family of proteins that mediate various cellular processes including cell proliferation and central nervous system (CNS) development, can be activated by Pb^{2+} at subnanomolar concentrations [25, 26] which may result in Pb^{2+}-induced neurotoxicity. Calmodulin (CaM) is another Ca^{2+}-binding protein that has previously been identified as playing a potential role in lead toxicity [24, 27], and ionic displacement was assumed to be the mechanism associated with toxicity as Pb^{2+} will occupy the Ca^{2+} binding sites in CaM with higher relative affinity than Ca^{2+} [28, 29]. CaM is a 148 residue, predominantly helical intracellular trigger protein (Fig. S1a) that responds to changes in cytosolic Ca^{2+} by binding up to four Ca^{2+} ions in two pairs of cooperative EF-hand sites [30]. The highly-conserved EF-Hand sites are comprised of a helix-loop-helix structure. Residues within the loop are identified by a relative position number 1–12, with binding of Ca^{2+} typically coordinated by residues in positions 1, 3, 5, 7, 9 and 12, where the coordinating ligand from position 7 is usually a carbonyl oxygen. CaM is divided into two structurally similar domains, each containing a pair of EF-Hand sites, separated by a trans-domain linker region comprising residues 76–84 (Fig. S1b). This region appears helical (Fig. S1c) in X-ray structures [31, 32], and as a flexible loop in NMR solution structures [33, 34]. The intrinsic flexibility of this region (Fig. S1d) allows the two domains to adopt a closer conformation to one another in solution [35] and is believed to be functionally important to CaM's ability to bind peptides and interact with enzymes as a secondary messenger controlling multiple biological functions [34]. Therefore, activation of CaM-mediated target proteins is largely dependent on the Ca^{2+} binding process and Ca^{2+}-induced conformational change.

CaM is also one of the only proteins with crystal structure data available showing both the Ca^{2+}- and Pb^{2+}-bound states (Fig. S1e and Fig. S1f) [36, 37]. Previous studies related to lead toxicity have reported that Pb^{2+} binding to CaM resulted in drastically altered downstream activity, displaying an initial increase (i.e., activation) and subsequent decrease (i.e., inhibition) for both CaM-sensitive phosphodiesterase (PDE) [22, 38] and myosin light-chain kinase (MLCK) [39]. However, it was not clear how Pb^{2+} or other toxic metals could activate and then subsequently deactivate these processes solely by ionic mimicry, indicating gaps in our understanding of the mechanism associated with lead molecular toxicity. Additionally, the presence of secondary cationic binding sites in CaM [40, 41] has not received detailed attention in discussions regarding lead toxicity, although a statistical analysis completed in our laboratory of Pb^{2+}-bound protein structures in the Protein DataBank (PDB) suggested that Pb^{2+} exhibits more flexible requirements for binding than

Ca^{2+} and will bind proteins outside of the known Ca^{2+}-binding sites. These apparent inconsistencies led us to hypothesis that lead molecular toxicity may be related to opportunistic binding of Pb^{2+} in secondary sites, such as the central helix of CaM, resulting in conformational changes that alter or inhibit protein activity [42]. Such an opportunistic binding model would have important human health implications as it would indicate a much broader pool of potential molecular targets for Pb^{2+} that would better explain the systemic effects observed with lead toxicity.

To test this hypothesis, CaM binding with Ca^{2+} and Pb^{2+} was evaluated using fluorescence spectroscopy and multidimensional high resolution NMR with ^{15}N-labeled protein. The effect of Pb^{2+} on Ca^{2+}/CaM was further examined by titrating Pb^{2+} into Ca^{2+}-saturated CaM using heteronuclear single quantum coherence (HSQC) NMR, heteronuclear $\{^{1}H, ^{15}N\}$ nuclear Overhauser effect (NOE) and NMR relaxation studies.

The results of this study demonstrated that Pb^{2+} alters the conformation of CaM in the Ca^{2+}-bound state, especially at the molecular recognition site, and provides evidence that molecular toxicity may be induced in CaM or other proteins as a result of binding opportunistically in secondary sites. This allosteric mechanism suggests that the promiscuous nature of Pb^{2+} allows for multiple molecular targets and by extension offers a comprehensive explanation for the resulting systemic pathology of lead toxicity.

2 Materials and Methods

2.1 Metal Standards

Ca^{2+} was obtained from Ionplus calcium standard (Orion Research Inc., Beverly, MA). Pb^{2+} was purchased as $Pb(NO_3)_2$ (Fisher Scientific, Fair Lawn, NJ) and prepared in ultra milli-Q double deionized water (ddH_2O, resistivity = 18.0 MΩ·cm).

2.2 Expression and purification of wild-type calmodulin (wt-CaM)

Recombinant rat wt-CaM (hereafter referred to as CaM) was expressed in *Escherichia coli* strain BL21(DE3)pLysS. CaM from rat was selected as it shares 99% sequence identity with human CaM. Expression and purification for homonuclear and ^{15}N-labelled proteins in either LB or minimal media followed previously reported protocols [43]. Final concentrations of the proteins were determined by measuring absorbance at 277 nm, and calculating concentration based on the Beer-Lambert Law where the molar absorptivity (ε) for CaM = 3030 M^{-1} cm^{-1} [44].

Buffers were treated with Analytical Grade Chelex 100 resin, 100–200 mesh Sodium Form (Bio-Rad Laboratories, Hercule, CA), to selectively remove divalent cations (e.g., Ca^{2+}). Protein samples were treated by passage through a small column packed with 2g polystyrene BAPTA (Invitrogen Molecular Probes, Eugene, OR), commercially referred to as Calcium Sponge***TM*** S, which has a reported approximate K_d for Ca^{2+} of 300 nM. Unless otherwise specified, all protein samples were prepared in high salt (100 mM KCl) environments, which were found in preliminary studies to have only minimal effect on Pb^{2+}-binding, and experiments were conducted at 37 °C in an effort to mimic physiological conditions as closely as possible.

2.3 Fluorescence studies

Fluorometric spectral analyses were conducted in triplicate using a PTI (Photon Technology International, Birmingham, NJ) spectrofluorometer equipped with a 75 W xenon arc lamp and a model 814 photomultiplier tube (PMT) detector. Samples were evaluated in 1 cm path

length quartz cuvettes at 21 °C. Protein sample concentrations were 10 μM in 800 μL, prepared in Chelex-treated buffers of 10 mM Tris pH 7.4, 100 mM KCl.

Previous work with CaM has demonstrated that the distributions of phenylalanine in the N-terminal domain and tyrosine in the C-terminal domain (Fig. S1a) provides a means to monitor binding of Ca^{2+} ions based on changes in the intrinsic fluorescence of these residues [45, 46]. While this approach cannot provide quantitative data for individual binding sites, it can provide macromolecular dissociation constants (K_d) for the individual domains.

Emission spectra for phenylalanine fluorescence were collected from 265–285 nm (3 nm excitation (Ex) slit widths, 4 nm emission slit widths, λ_{Ex} = 250 nm, integration 0.2 s, stepsize 1 nm). Emission spectra for tyrosine fluorescence were collected from 290–350 nm (2 nm excitation slit widths, 3 nm emission slit widths, λ_{Ex} = 277 nm, integration 0.2 s, stepsize 1 nm).

In this study, K_d values based on total metal concentration for direct titrations were calculated from the mean and standard deviation of triplicate experiments using Eq. 1, where $[P]_T$ is total protein concentration, $[M]_T$ is total metal concentration, and F is the fluorescence intensity.

$$F=\frac{([P]_T+[M]_T+K_d)-(([P]_T+[M]_T+K_d)^2-4[P]_T[M]_T)^{1/2}}{2[P]_T} \quad \text{(Eq. 1)}$$

$$K_{dM2}=\frac{(K_{app})(K_{dM1})}{((K_{dM1})+[M_1]_T)} \quad \text{(Eq. 2)}$$

$$K_{dM1}=\frac{([M_1]_T(K_{dM2}))}{((K_{app})-(K_{dM2}))} \quad \text{(Eq. 3)}$$

For competitive titrations involving pre-equilibration of the protein with one metal followed by titration with a second metal, the K_d in Eq. 1 becomes an apparent K_d (K_{app}). In Eq. 2, the K_d for a titrant metal (K_{dM2}) can be obtained based on K_{app} from Eq. 1, the known K_d for the pre-equilibrated metal ion (K_{dM1}) and the fixed, total concentration of the pre-equilibrated metal ion $[M_1]_T$ [47]. For titrations where the K_d of the titrant metal is known but not the pre-equilibrated metal, Eq. 2 is rearranged as Eq. 3. Alternatively, for titrations of Ca^{2+} to CaM which involve cooperative binding, data were fit using the Hill equation (Eq. 4), where *n* is the Hill coefficient. The free Ca^{2+} concentration was determined by competitive titration with Oregon Green indicator dye using a calcium buffering system (ethylene glycol tetraacetic acid (EGTA) combined with nitrilotriacetic acid (NTA)) [48].

$$Y=\frac{([M]_{Free})^n}{(([M]_{Free})^n+(K_d)^n)} \quad \text{(Eq. 4)}$$

2.4 NMR Analysis

All spectra were acquired on a 600 MHz Varian NMR spectrometer. Conversions of free induction decay (FID) files from Varian to Sparky formats were completed using NMRPipe [49] software. Peak assignment and area integration for 2D and 3D spectra were processed using Sparky software (T.D. Goddard, University of California, San Francisco, CA). Data

were analyzed or compiled in Microsoft Excel (Microsoft, Redmond, WA), while curve-fitting was completed using Kaleidagraph software (Synergy Software, Reading, PA). NMR sample tubes were purchased from Wilmad-Labglass (Vineland, NJ). D_2O (99.96%) was purchased from Cambridge Isotope Laboratories (Andover, MA).

2.5 2D NMR

The 500 μL samples for evaluation of both Ca^{2+} and Pb^{2+} by HSQC NMR were comprised of 253–400 μM ^{15}N-labeled CaM in 10 mM Bis-TRIS pH 6.5, with 5 mM 2-(N-morpholino)ethanesulfonic acid (MES) buffer, 10% D_2O, and 0.1 mM NaN_3 to inhibit bacterial growth. Samples were analyzed on a 600 MHz Varian NMR spectrometer using the N15 gradient enhanced heteronuclear single quantum coherence pulse sequence (gNHsqc) at 37 °C. Typically a total of 32 dummy scans and 32 acquisition scans were collected across a spectral width of 8384.9 Hz in the proton dimension, with 128 increments across a spectral width of 2000 Hz in the nitrogen dimension. Reference spectra for Ca^{2+}-free or Ca^{2+}-loaded CaM were acquired by treating samples first either with 10 mM EGTA or 20 mM Ca^{2+}. Three titration experiments were completed to monitor structural changes in CaM associated with metal binding. First, HSQC spectra were acquired for CaM with 0, 1, 2, 3, 4 and 6 molar equivalents (MEs) of Ca^{2+}. Similarly, HSQC spectra were acquired for CaM with 0, 1, 2, 3, 4, 5 and 6 MEs Pb^{2+}. Finally, HSQC spectra were obtained for the addition of 0.5, 1.0, 1.5, 2.0, 2.5 and 3.0 MEs Pb^{2+} to CaM presaturated with 6 MEs Ca^{2+} to evaluate structural changes associated with competitive binding. Due to sample precipitation problems, we were unable to add more than 3.0 MEs of Pb^{2+} to CaM samples presaturated with Ca^{2+}. Total chemical shift changes (Δδ) across both dimensions (^{15}N and ^{1}H) were weight-averaged based on Eq. 5. Peaks in the spectra for Ca^{2+}-free and Ca^{2+}-loaded CaM were assigned based on 3D HNCA assignment at 37 °C with previous assignments for Ca^{2+}-free CaM at 23 °C [50], and Ca^{2+}-loaded CaM at 37 °C [51].

$$\Delta\delta_{Total} = \sqrt{\frac{(\Delta\delta_{NH})^2 + \left(\frac{\Delta\delta_N}{5}\right)^2}{2}} \quad \text{(Eq. 5)}$$

2.6 Protein Dynamics

To compare dynamic properties of CaM complexed with either Ca^{2+} or both Ca^{2+} and Pb^{2+}, heteronuclear NOE data were collected and analyzed following the approach described by Seifert [52]. Samples consisted of 1.14 mM ^{15}N-labeled CaM prepared in 10 mM Tris pH 6.6, 100 mM KCl, 100 μM NaN_3, and 10% D_2O. For analysis of Ca^{2+}-loaded CaM, 20 mM Ca^{2+} was added to the sample. For analysis of Pb^{2+}, 2 MEs of Pb^{2+} was added to CaM pre-loaded with 6 MEs Ca^{2+}. Both analyses were run at 37 °C.

For NOE data, two experiments were conducted with ^{1}H saturation times of 0.0 and 4.0 s using pulse sequence gNnoe. Data for NOE were processed as a ratio (Eq. 6) where t4 and t0 are the integrated peak areas for relaxation times of 4s and 0s respectively.

$$R_{NOE} = \left(\frac{t4}{t0}\right) \quad \text{(Eq. 6)}$$

3 Results

3.1 Domain-specific binding affinities of CaM determined by intrinsic fluorescence

Changes in fluorescent intensities for Phe at 265–285 nm (excited at 250 nm) and Tyr at 290–350 nm (excited at 277 nm) as functions of metal concentration for both Ca^{2+} and Pb^{2+} binding with CaM are presented in Fig. 1, and the calculated dissociation constants are summarized in Table 1.

Calculated K_d values for Ca^{2+} for both the N-terminal (11.50±0.68 μM) and C-terminal (2.04±0.02 μM) domains were consistent both with reported values [48] and with known Ca^{2+} intracellular concentrations in the μM range.

Direct titration of Pb^{2+} to CaM produced a decrease in Phe fluorescence (Fig. 1b), similar to the response observed with Ca^{2+} (Fig. 1a). Curve-fitting of data using Eq. 1 produced a calculated K_d of 1.40±0.30 μM for binding of Pb^{2+} in the N-terminal domain which was as much as 8-fold higher than Ca^{2+} (Table 1).

Unlike the increase in Tyr fluorescence observed in Ca^{2+} titrations (Fig. 1a), the direct titration of Pb^{2+} produced a biphasic response characterized by a rapid initial increase in fluorescence intensity up to ~2:1 MEs of Pb^{2+}/Protein, followed by a hyperbolic decrease in intensity reaching a minimum below 10 MEs of Pb^{2+} (Fig. 1c). The initial increase (Phase 1, Fig. 1d) which mimics the Ca^{2+} response and peaks at ~2 MEs of Pb^{2+}, was interpreted as binding of Pb^{2+} in one of the two binding sites EF-III or EF-IV, while the subsequent decrease (Phase 2, Fig. 1e) was interpreted as binding in the other C-terminal domain site. Curve-fitting of data, based on Eq. 1, produced a calculated K_d of 0.73 ± 0.10 μM for Phase 1 and a K_d of 1.93 ± 0.32 μM for Phase 2 (Table 1). Interestingly, this value and the associated curve of the second phase in the tyrosine titration (Fig. 1e) are nearly identical to the corresponding curve and calculated K_d observed for the Phe signal change for the N-terminal domain. These results suggest a single higher affinity Pb^{2+}-binding site in the C-terminal domain and nearly equivalent affinity for the three remaining sites.

Competitive titrations to analyze changes in Tyr fluorescence were also conducted by presaturating CaM with Ca^{2+} followed by titration with Pb^{2+}, however, no change in fluorescence intensity was observed using this approach (data not shown), suggesting that Pb^{2+} does not displace Ca^{2+} in the C-terminal domain sites, or may do so with slow kinetics. Based on these results, 10 μM samples of Ca^{2+}-free CaM were pre-equilibrated with 20 μM Pb^{2+}, assuming that all Pb^{2+} was binding to the high affinity C-terminal domain sites, followed by titration of Ca^{2+}. The resulting data is still fit with Eq. 1, but the K_d value returned for Pb^{2+} is calculated by rearranging Eq. 2 into Eq. 3, and solving for K_{dm1} based on the known K_d for Ca^{2+} (K_{dm2}), K_d from Eq. 1 which becomes K_{app}, and the total, fixed concentration of Pb^{2+} pre-equilibrated with the protein $[M_1]_T$. Results indicated a K_d (K_{dm1}) of 0.67±0.06 μM (Table 1), which overlaps the standard deviation reported for results obtained by direct titration of Pb^{2+} (Fig. 1d).

3.2 Monitoring CaM binding with Pb^{2+} by NMR

Analyses of spectra for the titration of Ca^{2+} to apo-CaM indicates a domain-specific pattern of chemical exchange for rat CaM, consistent with results published by Jaren *et al.* for paramecium CaM [33]. At low concentrations of Ca^{2+} we observe peak loss due to broadening associated with intermediate chemical exchange, and the appearance of new peaks as a result of slow chemical exchange (Fig. 2a). These changes in the spectra contrast sharply with fast chemical exchange as seen with G59 and G23 (Fig. 2b) indicating single, averaged peaks transient in the spectra in response to Ca^{2+}-binding. In Fig. 2c we color-labeled the residues based on fast (blue), intermediate (purple) or slow (red) chemical

exchange, which demonstrates that slow and intermediate exchange occur almost exclusively in the C-terminal domain, with fast exchange observed primarily in the N-terminal domain. A summary of residues and their associated chemical exchange can be found in Table S1.

By comparing the spectra from the Ca^{2+}-free to the Ca^{2+}-loaded states, the magnitude of the absolute δ change (i.e., change in chemical shift across both the ^{1}H and ^{15}N dimensions from the initial δ values) reveals that the most significant changes occur for residues within the Ca^{2+}-binding sites (Fig. 3a), while comparatively small changes are observed in the linker region. For the titration of Pb^{2+} to CaM, some loss of signal is apparent as a number of peaks observed in the Ca^{2+} spectrum fail to reappear following addition of Pb^{2+}. However, from the peaks that are assigned, it is clear that the same trend is observed with addition of Pb^{2+}, with the most significant changes observed in the canonical EF-Hand sites (Fig. 3b).

We can also establish a relative order of occupancy for Ca^{2+} by (1) comparing total Δδ across both dimensions for successive points in the titration (Fig. 4) or (2) plotting the order in which signals disappear relative to MEs of Ca^{2+} added (Fig. S2). Based on the relative magnitude of Δδ between points in the titration in Fig. 4, we can observe that Ca^{2+} first binds in the C-terminal domain followed by the N-terminal domain sites. Moreover, binding of Ca^{2+} in one domain is accompanied by structural changes in the opposite domain. Chemical shift changes from 0–2 MEs Ca^{2+} (Fig. 4), corresponding to binding in the C-terminal domain, also produce structural changes in the N-terminal domain.

From 2–3 MEs Ca^{2+}, more restructuring is seen in the N-terminal domain due to binding in either site EF-I or EF-II, but is still accompanied by changes in the C-terminal domain. From 3–4 MEs Ca^{2+}, chemical shift changes indicate restructuring in both domains. The final, Ca^{2+}-saturated state of the protein was not observed until the addition of 6 MEs of Ca^{2+}, as determined by comparison with a reference spectrum obtained for 400 μM CaM in 20 mM Ca^{2+}. Similarly, the disappearance of critical signals in each of the binding sites occurred in a domain-specific order (Fig. S2) with peaks (highlighted in gray) disappearing first in the C-terminal domain followed by the N-terminal domain.

For Pb^{2+}, however, the order of occupancy could not be determined by analysis of Δδ which exhibited simultaneous changes in both domains (data not shown). However, from Fig. S2 we observe the most significant disappearance of peaks first in site EF-IV, followed by nearly-concurrent disappearance of peaks for residues in sites EF-I through EF-III. This is consistent with results of fluorescence analysis suggesting a single higher affinity Pb^{2+} site in the C-terminal domain with equivalent affinity for the three remaining sites.

The addition of Ca^{2+} sufficient to saturate CaM produces significant changes in the chemical shifts. Consistent with previous reports, we observed large changes in chemical shifts moving 4–8 ppm downfield in the spectra for I27, I63, I100 and V136 for Ca^{2+}-loaded CaM that were proposed to be related to cooperative binding between the paired binding sites in each domain [53]. Such changes, however, were not observed for binding of Pb^{2+}.

3.3 Titration of Pb^{2+} to Ca^{2+}-loaded CaM

The titration of Pb^{2+} to CaM presaturated with 6 MEs of Ca^{2+} produced interesting variations in the chemical shifts not observed with direct addition of Pb^{2+} to apo-CaM. Overlaying the HSQC spectra revealed significant movement of signals for key residues in or adjacent to the trans-domain linker region, specifically residues D78, D80, S81, E82, E83 and R86 (Fig. 5a). Analysis of absolute Δδ values (Fig. 3c) indicate displacement of Ca^{2+} by Pb^{2+} only in sites EF-I and EF-II, but not sites EF-III and EF-IV, as seen for residues G25

and G61 in Fig. 5b, which disappear following the addition of 0.5 MEs of Pb^{2+}. Also in Fig. 3c, the most significant structural changes occur in the linker region suggesting the presence of at least one additional binding site in this carboxyl-rich region of the sequence that is consistent with the coordination properties of Pb^{2+} binding [42].

Additionally, peaks for I27 and I63 disappear following addition of 0.5 MEs Pb^{2+}, which may indicate loss of intradomain cooperativity (Fig. 5c). However, peaks for I100 and V136 remain visible in the spectrum. These results strongly indicate that Pb^{2+} displaces Ca^{2+} only in the N-terminal domain sites EF-I and EF-II.

3.4 CaM:Pb dynamics

NOE data acquired for Ca^{2+}-saturated CaM (Fig. 6a) followed the same trends reported previously by Barbato [54], with increasing flexibility (i.e., less ordered secondary structure) apparent in the end termini, the central helix, and the small loop region separating sites EF-III and EF-IV.

Comparison of our NOE data between Ca^{2+}-loaded CaM in the absence (Fig. 6a) or presence (Fig. 6b) of 2 MEs Pb^{2+} suggests increased flexibility in sites EF-I and EF-II, but loss of flexibility in the linker region. Additionally, NOE values for residues in sites EF-III and EF-IV, while exhibiting more variance in the Pb^{2+}-bound protein, do not indicate any significant change in these regions, further indicating that Pb^{2+} does not displace Ca^{2+} in these sites.

4 Discussion

In some instances, metal toxicity has been explained by ionic mimicry, the primary mechanism associated with several types of metal toxicity [12]. Since oxygen ligands from proteins for Ca^{2+} binding can also be used as ligand atoms for different toxic metal ions, it was speculated that the effects of these toxic metal ions are mainly due to displacement of Ca^{2+} in different CaBPs [20–26] including CaM, CaM-activated skeletal muscle troponin C (TnC) [55], PKC [26], and synaptotagmin [2]. However, there is no direct proof of the theory of ionic mimicry and the observed biphasic contradictory behavior of Pb^{2+} binding cannot be adequately addressed by this theory [38, 39, 56–59]. Additionally, the presence of secondary cationic binding sites suggests potential alternatives to ionic mimicry as a mechanism of toxicity. To understand the molecular mechanism for lead toxicity, previous studies using different experimental approaches reported that CaM and other Ca^{2+}-binding proteins exhibit relatively higher binding affinities for Pb^{2+} compared with Ca^{2+}. Fullmer *et al*., using radioisotopes of Ca^{2+} and Pb^{2+} and equilibrium dialysis to facilitate binding, reported that chick CaBP initially binds 3–4 MEs of Pb^{2+} in preference to Ca^{2+} with a K_d of 1.1×10^{-6} M, and 1–2 additional MEs of Pb^{2+} with a K_d of 7×10^{-4} M [21]. Similar higher affinity was reported for binding of Pb^{2+} to both CaM and troponin C, however, these results were based on determined binding stoichiometries of 4.7 and 4.9 (Pb:Protein) for CaM and troponin C, and were reported as relative affinities rather than calculated dissociation constants. These reported stoichiometries support the existence of an additional Pb^{2+}-binding site for both CaM and troponin C which each have four Ca^{2+} binding sites. In another study, Aramini *et al*. [28] used 207Pb NMR to demonstrate binding of Pb^{2+} in the four EF-hand binding sites of CaM with higher relative affinity than Ca^{2+}. Similarly, NMR studies using ^{15}N labeled Gly residues in CaM by Ouyang and Vogel led them to report concurrent, high-affinity binding of Pb^{2+} in CaM's four EF-hand sites [29], however, further site-specific binding information could not be provided by this study due to precipitation of the samples beyond the 2:1 Pb^{2+}:CaM ratio, and dynamic properties were not reported. Nevertheless, these reported studies suggest that an alternative mechanism of toxicity beyond simple ionic displacement exists. Therefore, there is a need to fill in the gaps in our

understanding of the molecular mechanism associated with molecular metal toxicity and the structural properties associated with their interactions with proteins.

4.1 Differential domain specific Ca^{2+} and Pb^{2+} binding affinities of CaM

The method of determining domain level binding affinities was used in our study and in previous studies because the cooperative binding of Ca^{2+} in the paired EF-hand sites of CaM precludes a precise determination of affinity in the individual sites. When individual affinity values have been reported, they were obtained either by mutations to deactivate one of the paired sites [60], calculated theoretical affinities based on thermodynamic models [61], or by probing site-specific binding by grafting EF-hand binding sites into a scaffold protein [62]. Alternatively, domain-specific affinity values may be obtained via changes in intrinsic fluorescence [48]. Using intrinsic fluorescence signals from Tyr and Phe, we were able to compare the metal binding affinities for Ca^{2+} and Pb^{2+} at the domain level, showing that CaM exhibits a higher relative affinity (~8-fold) for Pb^{2+} over Ca^{2+} in the N-terminal domain with a smaller comparative increase (~3-fold) in the C-terminal domain (Table 1). However, the binding affinity for Pb^{2+} in the N-terminal domain is only ~2-fold higher than that observed for Tyr Phase 1 binding in the C-terminal domain, and equivalent to the calculated K_d for tyrosine Phase II binding (Fig. 1c), which suggests a single, marginally-higher affinity binding site in the C-terminal domain, with the three remaining sites exhibiting approximately equivalent binding affinities. The biphasic response to Pb^{2+} in the C-terminal domain differs significantly from results reported for binding of Ca^{2+}. We interpreted this biphasic response as two distinct binding events in the paired EF-hand sites, as this was consistent with our NMR data. However, it is also possible that binding of 2 Pb^{2+} ions is represented only by the initial fluorescence increase up to 2 MEs of Pb^{2+}, and that the decrease observed in the second phase represents fluorescence quenching due to conformational changes induced by binding of Pb^{2+} in the central helix or elsewhere.

Similarly, analyses of HSQC data using ^{15}N-labelled CaM revealed the disappearance of peaks for residues G61, G132 and G134 at 1 MEs Pb^{2+}, followed by the disappearance of G23, G59, and G96 at 2 MEs Pb^{2+}. Signals for residues G23, G61, and G96 subsequently reappeared in the spectra with increasing Pb^{2+} concentration (i.e., slow exchange), while signals for residues G25 and G98 remained visible across the spectra. These residues are important because they reside in the loop regions of the EF-hand sites (I through IV). In this study, the initial disappearance of residues G132 and G134 (Fig. S2) at one ME Pb^{2+} in Ca^{2+}-free CaM suggests binding first in site EF-IV, followed by a concurrent distribution of Pb^{2+} across sites EF-I through EF-III, consistent with results acquired through fluorescence studies. Also consistent with our findings, Ouyang and Vogel, using ^{15}N-labeled Gly, monitored binding of Pb^{2+} in the four EF-hand sites based on the disappearance of signals for G23 and G25 (EF-I), G59 and G61 (EF-II), G96 and G98 (EF-III) and G132 and G134 (EF-IV), for one and then two MEs of Pb^{2+} [29]. However, these studies were limited by sample precipitation reported beyond two MEs of Pb^{2+}, and some of the minor differences reported by Ouyang and our study may be attributed to our use of a higher field strength NMR spectrometer and variations in our experimental approach. Additionally, our results provide quantitative data on binding constant values (Table 1).

4.2 Differential binding effect on EF-hand binding sites

Analysis of the HSQC spectra in this study provides a possible explanation for the similar binding affinities between Pb^{2+} and the EF-hand CaM Ca^{2+}-binding sites, based on the disappearance of signals for residues I27 and I63 (Fig. 5c). These residues occupy position 8 in the EF-loop sequence. Previous NMR studies reported by Biekofsky *et al.* [53] indicated that Ca^{2+} binding with the loop position 7 ligand results in observed deshielding (+4 to +8 ppm) of the mainchain nitrogen in position 8 due to polarization of the O(7)=C(7)-N(8)

amido group, which was used to monitor occupancy of Ca^{2+} in CaM, and provide evidence of cooperativity between the paired EF-Hand sites. It is possible that the disappearance of signals for these residues following addition of Pb^{2+} may indicate conformational changes resulting in disruption of cooperativity between paired binding sites, particularly in sites EF-I and EF-II. A structural basis for this conformational change may be observed in the crystal structures of Pb^{2+}-bound CaM 1n0y.pdb and 2v01.pdb (Fig. S1e and Fig. S1f), where the T26 O^{γ} oxygen appears to rotate inward, placing it close enough (~3.5 Å) to the Pb^{2+} ion to serve as an active coordinating ligand in addition to the carbonyl oxygen utilized in binding of Ca^{2+} (Fig. S3).

Our results and others suggest only minimal deviation in binding affinities between Pb^{2+} and the four EF-hand Ca^{2+}-binding sites in CaM, which would imply non-preferential occupancy between equivalent sites. Conversely, Ca^{2+} first occupies the higher affinity C-terminal domain EF-hand sites in CaM, followed by occupancy of the N-terminal domain sites [63]. Additionally, binding of Ca^{2+} in each domain involves cooperativity between the paired EF-Hand sites [64, 65] which is believed to be due to the formation of a short β-sheet between residues in position 8 of the paired EF-Loops joining EF-I with EF-II, and EF-III with EF-IV [66, 67]. Loss of cooperativity between the EF-Hand pairs, as suggested by structural differences between the two metals, would provide a plausible explanation for the similar affinities between Pb^{2+} and the four EF-Hand sites in CaM.

4.3 Differential structural and dynamic changes upon Ca^{2+} and Pb^{2+} binding

In this paper, we provide evidence to suggest a unique binding mode for Pb^{2+} contingent upon Ca^{2+}-induced protein folding. As seen in Fig. 3c, the addition of Pb^{2+} to Ca^{2+}-loaded CaM results in the disappearance of signals exclusively in sites EF-I (D22, G25 and I27) and EF-II (D56, A57, G61, I63, and E67). Conformational change due to binding is further revealed in the movement of signals in the spectra (Fig. 5), particularly in sites EF-I, EF-II, and the linker region, as plotted in Fig. 3c. These results are closely correlated with our analyses of NOE data which indicate that the addition of Pb^{2+} to Ca^{2+}-loaded CaM apparently results in loss of flexibility in sites EF-I, EF-II and the linker region (Fig. 6), while residues in sites EF-III and EF-IV appear unperturbed. These data suggest that Pb^{2+} displaces Ca^{2+} only in the N-terminal domain sites EF-I and EF-II, and we can speculate that the positive cooperativity associated with Ca^{2+}-binding between the paired sites EF-III and EF-IV [64, 65] in the C-terminal domain is sufficient to inhibit translocation of Pb^{2+} into the sites, while the 8-fold higher affinity of CaM for Pb^{2+} compared with Ca^{2+} in the N-terminal domain is sufficient for Pb^{2+} to displace Ca^{2+}.

Furthermore, we observed significant δ change due to fast chemical exchange for residues in the linker with the addition of Pb^{2+} to the Ca^{2+}-bound protein (Fig. 3c), but not with the addition of Pb^{2+} to Ca^{2+}-free CaM. Moreover, Δδ values for residues in the linker exceed changes observed in sites EF-I and EF-II (Fig. 3c), which suggests that Pb^{2+} may bind opportunistically in this functionally-important region characterized by high electrostatic potential [42] due to a cluster of oxygen-rich sidechains (DTDSEEE) in positions 78–84. This argues for a unique binding mode observed only when CaM initially adopts an active Ca^{2+}-induced conformer which prevents structural reconfiguration in the C-terminal domain as a consequence of ionic displacement. It should be noted that data fitting of chemical shift perturbations in the central helix (Fig. 5a) could not be performed to determine binding affinity, as the samples were found to precipitate before the endpoint of the titration was reached, reflecting a common problem associated with Pb^{2+} solubility also reported by Ouyang [29].

The unique Ca^{2+} potentiated binding mode for Pb^{2+} with CaM proposed in this paper is supported by several previous studies. Shirran and Barran reported that Pb^{2+} affinity for

CaM increases relative to other divalent cations in the presence of Ca^{2+} [68]. Mills and Johnson reported that Pb^{2+} and other metals may bind to Ca^{2+}-bound CaM in secondary sites forming an allosterically potentiated conformer [69], while Raos and Kasprzak suggested the existence of two secondary binding sites occupied by Ni^{2+} in the Ca^{2+}-bound state [70]. Similarly, a study by Milos *et al.* [41] presents compelling evidence that Zn^{2+} interacts with CaM not through the four EF-Hand sites, but by binding in six secondary sites with nearly equivalent affinity. Milos further concluded, based on changes in enthalpy, that binding of Zn^{2+} and Mg^{2+} in these secondary sites allosterically antagonizes binding of Ca^{2+} in the EF-Hand sites, and vice-versa. Binding of Pb^{2+} in one or more of these secondary binding sites could produce the antagonistic effects described by Milos which could explain the biphasic tyrosine response to Pb^{2+} (Fig. 1c), Pb^{2+}-induced global conformational changes, and the inhibition of CaM activity at higher concentrations of Pb^{2+}.

It is worth noting that none of these cited studies identified the locations of these secondary sites in CaM, however, strong evidence exists to support our conclusion that at least one of these sites can be found in the central linker of CaM. Bertini *et al.* [40] reported a potential metal-binding site in the linker region of CaM based on the disappearance of key NMR signals (residues 78–81) following addition of 0.3 MEs of Yb3+, and Kursula and Majava [36] identified a Ca^{2+}-binding site in the linker chelated by residues R74 and D78 in the crystal structure of Pb^{2+}-bound to human CaM.

Binding of Pb^{2+} in this region is consistent with our previously published study indicating that Pb^{2+} can bind to carboxyl and hydroxyl groups in regions lacking defined binding geometries yet characterized by high electrostatic potential [42], such as the cluster of oxygen-rich sidechains (DTDSEEE) in positions 78–84.

It is also possible that the observed changes in the linker occur in response to binding in some region of the protein more distant from the linker. The Pb-CaM structure reported by Kursula and Majava [36] depicts binding of Pb^{2+} by carboxyl groups from D118 and D122, and significant chemical shift changes (>0.05δ) are observed in our data for residues T117 and R126 (Fig. 3c) as a result of Pb^{2+}-binding. The residue sequence 117–123 (Fig. S1a) includes a group of carboxyl-rich sidechains (TDEEVDE) that could potentially bind Pb^{2+}. However, unlike the proposed binding sites in the linker, these residues are all found in an α–helix, and unless the helix itself were to unwind, which was not indicated in the analysis of our dynamic NMR data, this explanation appears less likely as it is not clear how binding in this region would induce major conformational changes in the linker region.

4.4 Implication for activation of CaM

A study by Chao *et al*. reported that Pb^{2+} exhibited a biphasic effect on the amount of phosphate transferred from [γ-^{32}P] ATP into MLCK, with stimulation observed at low concentrations followed by inhibition at higher concentrations [56]. Similarly, Habermann observed that Pb^{2+}-bound CaM initially activates PDE with higher potency than Ca^{2+}, but increasing Pb^{2+} concentration subsequently inhibited CaM-dependent phosphorylation [38].

From these functional assays and structural studies, it is likely that at low concentrations of Pb^{2+}, Pb^{2+} occupies the Ca^{2+}-binding sites in Ca^{2+}-free CaM. The nearly-equivalent binding affinity of CaM for Pb^{2+} likely results in multiple complex conformers, one or more resembling the Ca^{2+}/CaM complex in form and function [28, 29]. With increasing Pb^{2+} concentration, CaM eventually adopts a conformation which inhibits protein function.

Our proposed mechanism addresses the inhibitory effect of Pb^{2+} binding at higher concentrations as reported by both Chao [56] and Habermann [38]. The introduction of Pb^{2+} in this environment results in displacement of Ca^{2+} in sites EF-I and EF-II, coupled with

opportunistic binding in the electronegative central helix which alters the conformation of this region, thus inhibiting the ability of CaM to bind other target proteins. Increasing Pb^{2+} concentration presumably produces a more compact or dynamically-restricted conformer incapable of binding properly with target ligand molecules as was observed with osteocalcin [71]. The loss of functional plasticity in the central helix of CaM interferes with its ability to interact with downstream proteins. Mutating the glutamate cluster of residues 82–84 (EEE) to lysines was found to abolish or greatly impair activation of NAD kinase and MLCK respectively, but had no effect on phosphodiesterase [72]. Conversely, deletion of residues 79–80 (DTD) abolished activation of phosphodiesterase but had no effect on MLCK [73, 74].

5 Conclusions

Our results demonstrated that Pb^{2+} has higher binding affinity than Ca^{2+} for both the N- and C-terminal domains. Binding of Pb^{2+} results in structural changes distinct from the Ca^{2+}-bound state, and may disrupt the cooperativity observed between paired EF-hand sites during binding of Ca^{2+} [61, 63, 75]. Dynamic NMR studies suggested that Pb^{2+} displaces Ca^{2+} only in sites EF-I and EF-II, while the most significant chemical shift changes were observed in the carboxyl-rich linker region (residues 76–84). This provides strong evidence for opportunistic binding of Pb^{2+} outside of the known Ca^{2+}-binding sites and an alternative mechanism for structural changes in the protein. This mechanism is consistent with the reported concentration-dependent, biphasic activation and inhibition associated with Pb^{2+}-binding of CaM, and may account for the behavior of other toxic metals, such as lanthanides, observed to interact with CaM outside of the known Ca^{2+}-binding sites. Finally, these results suggest that systemic effects of toxicity resulting from exposure to lead or other metals may be due to interactions with multiple molecular targets rather than simple ionic displacement.

Supplementary Material

Refer to Web version on PubMed Central for supplementary material.

Acknowledgments

The authors would like to thank Natalie White for her critical reading of this paper. Funding for this work was in part provided by NIH Grants EB007268 and GM081749 to JJY, Georgia Research Alliance (Funding to GSU for Varian Inova 600 NMR), and a GSU Molecular Basis of Disease (MBD) fellowship to MK.

Abbreviations

ALAD	aminolevulinic acid dehydratase
BAPTA	1,2-bis(o-aminophenoxy)ethane-N,N,N'-N'-tetraacetic acid
CaBP	calcium binding protein
CaM	calmodulin
EGTA	ethylene glycol tetraacetic acid
HSQC	Heteronuclear Single Quantum Coherence
LB	lysogeny broth
ME	Molar Equivalent
MES	2-(N-morpholino)ethanesulfonic acid

MLCK	Myosin light-chain kinase
NTA	nitrilotriacetic acid
NOE	Nuclear Overhauser Effect
PDE	phosphodiesterase
PKC	protein kinase C
RNR	ribonucleotide reductase

References

1. Bressler J, Kim K-a, Chakraborti T, Goldstein G. Neurochem. Res. 1999; vol. 24:595–600. [PubMed: 10227691]
2. Bouton CM, Frelin LP, Forde CE, Arnold Godwin H, Pevsner J. J. Neurochem. 2001; vol. 76:1724–1735. [PubMed: 11259490]
3. Chetty CS, Reddy GR, Murthy KS, Johnson J, Sajwan K, Desaiah D. Int. J. Toxicol. 2001; vol. 20:113–120. [PubMed: 11488553]
4. Moore MR, Goldberg A, Yeung-Laiwah AA. Ann. N. Y. Acad. Sci. 1987; vol. 514:191–203. [PubMed: 3442384]
5. Aub JC, Reznikoff P. J. Exp. Med. 1924; vol. 40:189–208. [PubMed: 19868909]
6. Nolan CV, Shaikh ZA. Toxicology. 1992; vol. 73:127–146. [PubMed: 1319092]
7. Khalil-Manesh F, Gonick HC, Weiler EW, Prins B, Weber MA, Purdy RE. Am. J. Hypertens. 1993; vol. 6:723–729. [PubMed: 8110424]
8. Apostoli P, Bellini A, Porru S, Bisanti L. Am. J. Ind. Med. 2000; vol. 38:310–315. [PubMed: 10940969]
9. Ronis MJ, Badger TM, Shema SJ, Roberson PK, Templer L, Ringer D, Thomas PE. J. Toxicol. Environ. Health A. 1998; vol. 54:101–120. [PubMed: 9652547]
10. Hernandez-Ochoa I, Garcia-Vargas G, Lopez-Carrillo L, Rubio-Andrade M, Moran-Martinez J, Cebrian ME, Quintanilla-Vega B. Reprod. Toxicol. 2005; vol. 20:221–228. [PubMed: 15907657]
11. Johnson FM. Mutat. Res. 1998; vol. 410:123–140. [PubMed: 9637233]
12. Bridges CC, Zalups RK. Toxicol. Appl. Pharmacol. 2005; vol. 204:274–308. [PubMed: 15845419]
13. Bitto E, Bingman CA, Wesenberg GE, McCoy JG, Phillips GN Jr. J. Biol. Chem. 2006; vol. 281:20521–20529. [PubMed: 16672222]
14. Kim Y, Yoo CI, Lee CR, Lee JH, Lee H, Kim SR, Chang SH, Lee WJ, Hwang CH, Lee YH. Ind. Health. 2002; vol. 40:23–27. [PubMed: 11926511]
15. Bergdahl IA, Grubb A, Schutz A, Desnick RJ, Wetmur JG, Sassa S, Skerfving S. Pharmacol. Toxicol. 1997; vol. 81:153–158. [PubMed: 9353844]
16. Kelada SN, Shelton E, Kaufmann RB, Khoury MJ. Am. J. Epidemiol. 2001; vol. 154:1–13. [PubMed: 11427399]
17. Ballatori N. Environ. Health Perspect. 2002; vol. 110(Suppl 5):689–694. [PubMed: 12426113]
18. Simons TJ, Pocock G. J. Neurochem. 1987; vol. 48:383–389. [PubMed: 2432178]
19. Atchison WD. J. Bioenerg. Biomembr. 2003; vol. 35:507–532. [PubMed: 15000519]
20. Dowd TL, Rosen JF, Gundberg CM, Gupta RK. Biochim. Biophys. Acta. 1994; vol. 1226:131–137. [PubMed: 8204659]
21. Fullmer CS, Edelstein S, Wasserman RH. J. Biol. Chem. 1985; vol. 260:6816–6819. [PubMed: 3997849]
22. Goldstein GW, Ar D. Life Sci. 1983; vol. 33:1001–1006. [PubMed: 6310286]
23. Godwin HA. Curr. Opin. Chem. Biol. 2001; vol. 5:223–227. [PubMed: 11282351]
24. Goering PL. Neurotoxicology. 1993; vol. 14:45–60. [PubMed: 8247411]
25. Long GJ, Rosen JF, Schanne FA. J. Biol. Chem. 1994; vol. 269:834–837. [PubMed: 8288636]

26. Markovac J, Goldstein GW. Nature. 1988; vol. 334:71–73. [PubMed: 3386747]
27. Cox JL, Harrison SD Jr. Biochem. Biophys. Res. Commun. 1983; vol. 115:106–111. [PubMed: 6615519]
28. Aramini JM, Hiraoki T, Yazawa M, Yuan T, Zhang M, Vogel HJ. J. Biol. Inorg. Chem. 1996; vol. 1:39–48.
29. Ouyang H, Vogel HJ. Biometals. 1998; vol. 11:213–222. [PubMed: 9850564]
30. Kretsinger RH, Nockolds CE. J. Biol. Chem. 1973; vol. 248:3313–3326. [PubMed: 4700463]
31. Chattopadhyaya R, Meador WE, Means AR, Quiocho FA. J. Mol. Biol. 1992; vol. 228:1177–1192. [PubMed: 1474585]
32. Wilson MA, Brunger AT. J. Mol. Biol. 2000; vol. 301:1237–1256. [PubMed: 10966818]
33. Jaren OR, Kranz JK, Sorensen BR, Wand AJ, Shea MA. Biochemistry. 2002; vol. 41:14158–14166. [PubMed: 12450379]
34. Vogel HJ. Biochem. Cell. Biol. 1994; vol. 72:357–376. [PubMed: 7605608]
35. Heidorn DB, Trewhella J. Biochemistry. 1988; vol. 27:909–915. [PubMed: 3365370]
36. Kursula P, Majava V. Acta Crystallogr. Sect. F Struct. Biol. Cryst. Commun. 2007; vol. 63:653–656.
37. Wilson MA, Brunger AT. Acta Crystallogr. D Biol. Crystallogr. 2003; vol. 59:1782–1792. [PubMed: 14501118]
38. Habermann E, Crowell K, Janicki P. Arch. Toxicol. 1983; vol. 54:61–70. [PubMed: 6314931]
39. Chao SH, Bu CH, Cheung WY. Arch. Toxicol. 1995; vol. 69:197–203. [PubMed: 7717877]
40. Bertini I, Gelis I, Katsaros N, Luchinat C, Provenzani A. Biochemistry. 2003; vol. 42:8011–8021. [PubMed: 12834353]
41. Milos M, Comte M, Schaer JJ, Cox JA. J. Inorg. Biochem. 1989; vol. 36:11–25. [PubMed: 2746218]
42. Kirberger M, Yang JJ. J. Inorg. Biochem. 2008; vol. 102:1901–1909. [PubMed: 18684507]
43. Zhou Y, Yang W, Lurtz MM, Ye Y, Huang Y, Lee HW, Chen Y, Louis CF, Yang JJ. J. Biol. Chem. 2007; vol. 282:35005–35017. [PubMed: 17901047]
44. Wallace RW, Tallant EA, Cheung WY. Cold Spring Harb. Symp. Quant. Biol. 1982; vol. 46(Pt 2): 893–901. [PubMed: 6286224]
45. Sorensen BR, Shea MA. Biochemistry. 1998; vol. 37:4244–4253. [PubMed: 9521747]
46. VanScyoc WS, Sorensen BR, Rusinova E, Laws WR, Ross JB, Shea MA. Biophys. J. 2002; vol. 83:2767–2780. [PubMed: 12414709]
47. Yang JJ, Yang J, Wei L, Zurkiya O, Yang W, Li S, Zou J, Zhou Y, Maniccia AL, Mao H, Zhao F, Malchow R, Zhao S, Johnson J, Hu X, Krogstad E, Liu ZR. J. Am. Chem. Soc. 2008; vol. 130:9260–9267. [PubMed: 18576649]
48. Jiang J, Zhou Y, Zou J, Chen Y, Patel P, Yang JJ, Balog EM. Biochem. J. 2010; vol. 432:89–99. [PubMed: 20815817]
49. Delaglio F, Grzesiek S, Vuister GW, Zhu G, Pfeifer J, Bax A. J. Biomol. NMR. 1995; vol. 6:277–293. [PubMed: 8520220]
50. Kuboniwa H, Tjandra N, Grzesiek S, Ren H, Klee CB, Bax A. Nat. Struct. Biol. 1995; vol. 2:768–776. [PubMed: 7552748]
51. Torizawa T, Shimizu M, Taoka M, Miyano H, Kainosho M. J. Biomol. NMR. 2004; vol. 30:311–325. [PubMed: 15754057]
52. Seifert MH, Georgescu J, Ksiazek D, Smialowski P, Rehm T, Steipe B, Holak TA. Biochemistry. 2003; vol. 42:2500–2512. [PubMed: 12614144]
53. Biekofsky RR, Martin SR, Browne JP, Bayley PM, Feeney J. Biochemistry. 1998; vol. 37:7617–7629. [PubMed: 9585577]
54. Barbato G, Ikura M, Kay LE, Pastor RW, Bax A. Biochemistry. 1992; vol. 31:5269–5278. [PubMed: 1606151]
55. Chao SH, Bu CH, Cheung WY. Arch. Toxicol. 1990; vol. 64:490–496. [PubMed: 2148867]
56. Chao SH, Suzuki Y, Zysk JR, Cheung WY. Mol. Pharmacol. 1984; vol. 26:75–82. [PubMed: 6087119]

57. Kern M, Wisniewski M, Cabell L, Audesirk G. Neurotoxicology. 2000; vol. 21:353–363. [PubMed: 10894125]
58. Ferguson C, Kern M, Audesirk G. Neurotoxicology. 2000; vol. 21:365–378. [PubMed: 10894126]
59. Suzuki Y, Chao SH, Zysk JR, Cheung WY. Arch. Toxicol. 1985; vol. 57:205–211. [PubMed: 2998298]
60. Maune JF, Klee CB, Beckingham K. J. Biol. Chem. 1992; vol. 267:5286–5295. [PubMed: 1544911]
61. Linse S, Helmersson A, Forsen S. J. Biol. Chem. 1991; vol. 266:8050–8054. [PubMed: 1902469]
62. Ye Y, Lee HW, Yang W, Shealy S, Yang JJ. J. Am. Chem. Soc. 2005; vol. 127:3743–3750. [PubMed: 15771508]
63. Ikura M, Hiraoki T, Hikichi K, Mikuni T, Yazawa M, Yagi K. Biochemistry. 1983; vol. 22:2573–2579. [PubMed: 6683101]
64. Forsen S, Linse S, Drakenberg T, Kordel J, Akke M, Sellers P, Johansson C, Thulin E, Andersson I, Brodin P, Grundström T, Skelton N, Chazin W. Ciba Found. Symp. 1991; vol. 161:222–236. [PubMed: 1667634]
65. Hiraoki T, Vogel HJ. J. Cardiovasc. Pharmacol. 1987; vol. 10(Suppl 1):S14–S31. [PubMed: 2442507]
66. Biekofsky RR, Turjanski AG, Estrin DA, Feeney J, Pastore A. Biochemistry. 2004; vol. 43:6554–6564. [PubMed: 15157088]
67. Ishida H, Takahashi K, Nakashima K, Kumaki Y, Nakata M, Hikichi K, Yazawa M. Biochemistry. 2000; vol. 39:13660–13668. [PubMed: 11076504]
68. Shirran SL, Barran PE. J. Am. Soc. Mass. Spectrom. 2009; vol. 20:1159–1171. [PubMed: 19297189]
69. Mills JJ, S J. J. Biol. Chem. 1985; vol. 260:15100–15105. [PubMed: 4066663]
70. Raos N, Kasprzak KS. Fundam. Appl. Toxicol. 1989; vol. 13:816–822. [PubMed: 2620798]
71. Dowd TL, Li L, Gundberg CM. Biochim. Biophys. Acta. 2008; vol. 1784:1534–1545. [PubMed: 18793762]
72. Craig TA, Watterson DM, Prendergast FG, Haiech J, Roberts DM. J. Biol. Chem. 1987; vol. 262:3278–3284. [PubMed: 3029108]
73. Tabernero L, Taylor DA, Chandross RJ, VanBerkum MF, Means AR, Quiocho FA, Sack JS. Structure. 1997; vol. 5:613–622. [PubMed: 9195880]
74. VanBerkum MF, George SE, Means AR. J. Biol. Chem. 1990; vol. 265:3750–3756. [PubMed: 2154485]
75. Andersson A, Forsen S, Thulin E, Vogel HJ. Biochemistry. 1983; vol. 22:2309–2313. [PubMed: 6860630]

Highlights

- Pb^{2+} displaces Ca^{2+} in the N-terminal, but not the C-terminal domain, of calmodulin.
- Pb^{2+} binding affinity is only 3- to 8-fold higher than Ca^{2+} in Ca^{2+}-binding sites.
- Opportunistic binding of Pb^{2+} outside of Ca^{2+} sites alters protein conformation.
- Pb^{2+} toxicity may be due to opportunistic binding, rather than by displacement.

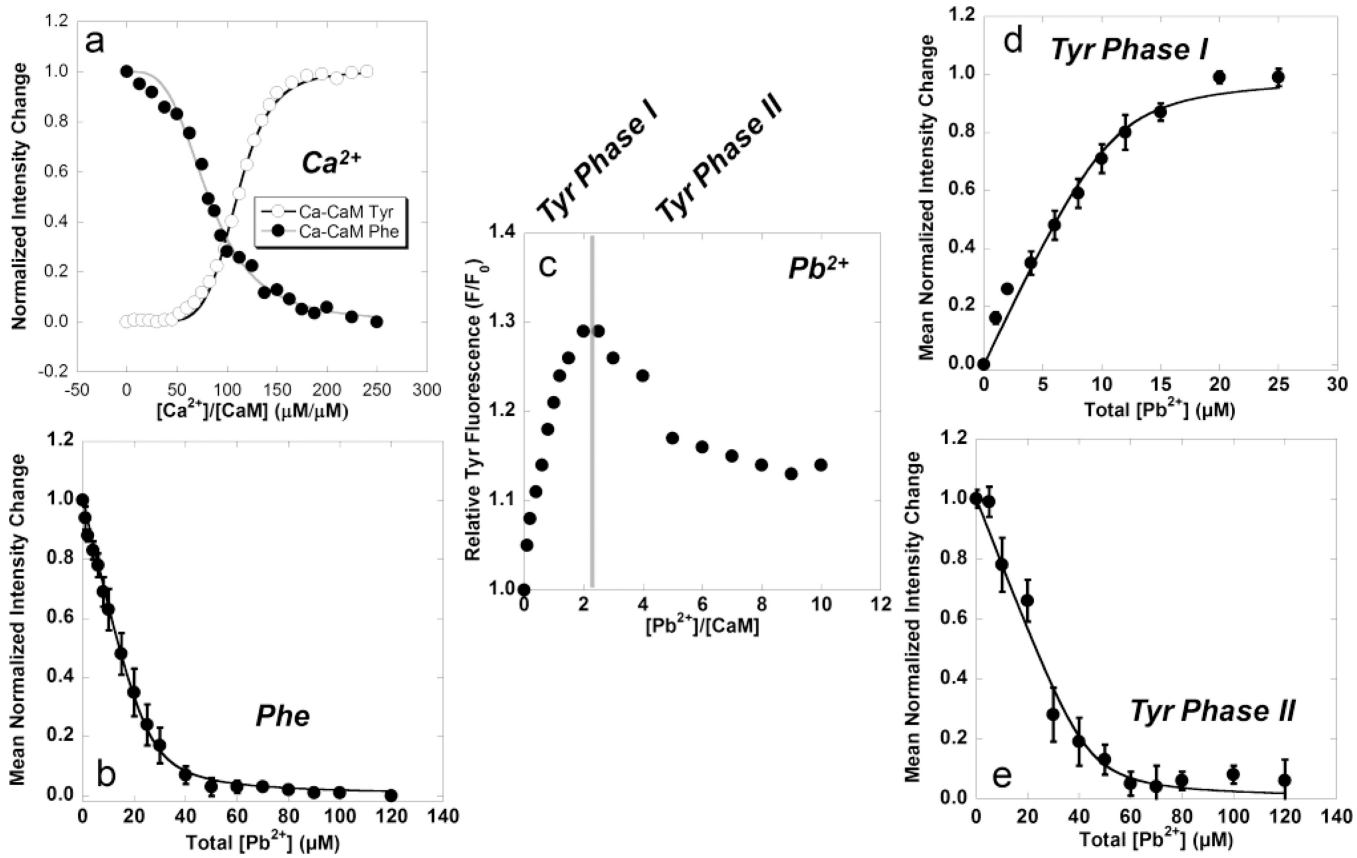

Fig. 1.

(**a**) Mean normalized Tyr (○) and Phe (●) fluorescence changes as a function of total [Ca^{2+}] using Eq. 4. (**b**) Mean normalized Phe fluorescence change as a function of total [Pb^{2+}] for the N-terminal domain with calculated K_d of 1.40 ± 0.30 μM. (**c**) Relative Tyr fluorescence as a function of Pb^{2+}:CaM complex formation. The observed biphasic fluorescent response is divided into (**d**) Phase 1 with a calculated K_d of 0.73 ± 0.10 μM and (**e**) Phase 2 with a calculated K_d of 1.93 ± 0.32 μM. The calculated K_d for Phase 2 of the Tyr fluorescence falls within the standard deviation calculated for Phe fluorescence in the N-terminal domain.

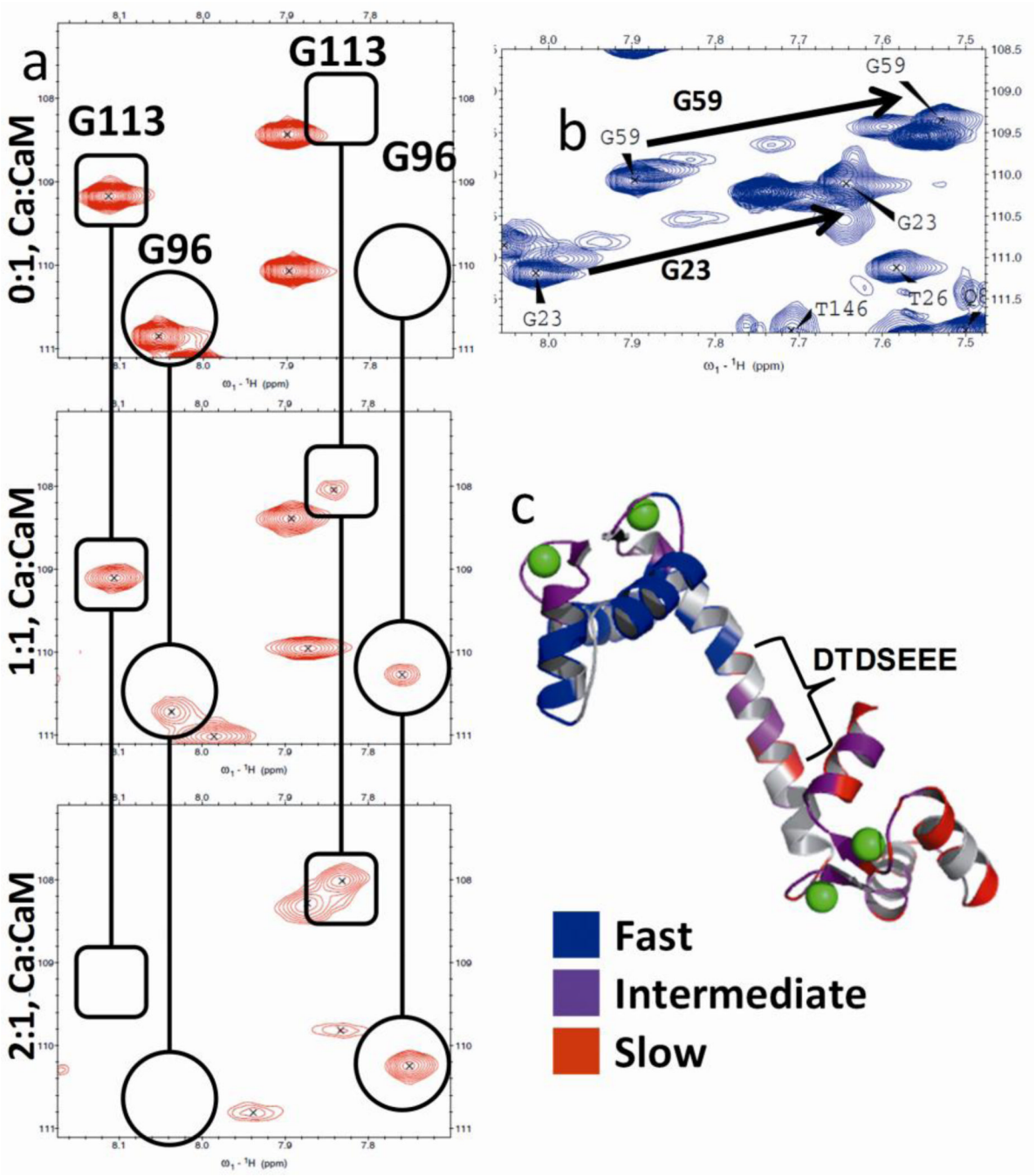

Fig. 2.

(**a**) Slow chemical exchange for G113 (in rounded rectangle) and G96 (in circle). Both residues display a single peak at 0 MEs Ca^{2+}, followed by the emergence of a second peak at 1 ME Ca^{2+}. At 2 MEs Ca^{2+}, the original peak in each pair is undetectable, leaving only the second peak. (**b**) Fast chemical exchange for G23 and G59. (**c**) CaM (3cln.pdb) with residues color-labeled to indicate fast (blue), intermediate (purple) and slow (red) chemical exchange. The carboxyl-rich central linker is highlighted in the bracket.

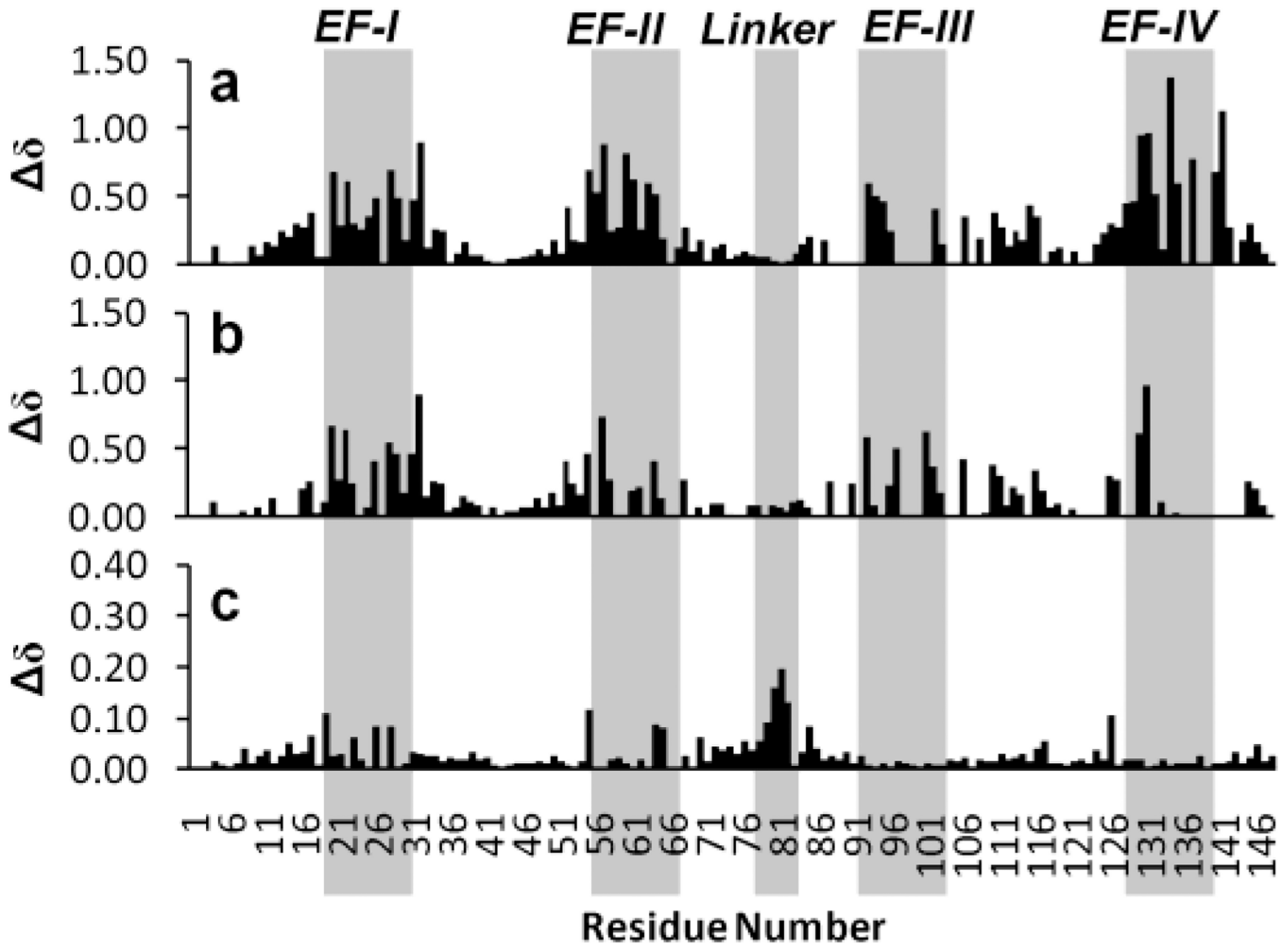

Fig. 3.

Weight-averaged chemical shift change (Δδ) in 15N HSQC spectra for titration of (**a**) Ca^{2+} and (**b**) Pb^{2+} complexed with CaM, and (**c**) Pb^{2+} added to Ca^{2+}/CaM complex. The EF-Hand sites and the linker region in the sequence are highlighted in gray. Some loss of data is observed in (**b**) for addition of Pb^{2+}, however, in both graphs the highest magnitude Δδ is clearly observed for residues within the four EF-Hand Ca^{2+}-binding sites, with minimal change observed in the linker region. In (**c**) Pb^{2+} displaces Ca^{2+} in sites EF-I and EF-II, while the most significant structural changes occur in the linker.

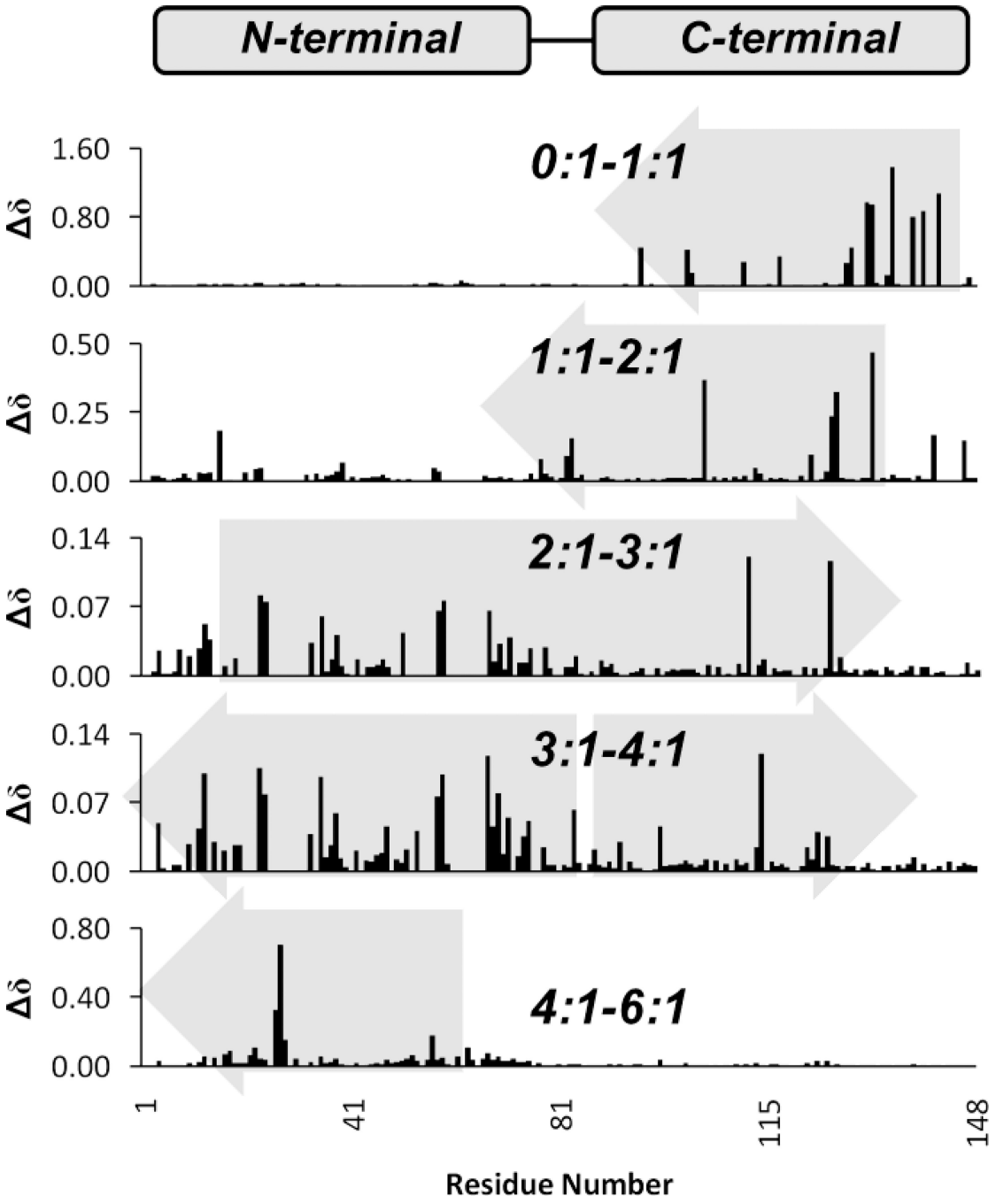

Fig. 4.

Absolute changes in δ between successive points in the titration of Ca^{2+} to CaM, where changes are expressed in molar ratios of Ca^{2+}:CaM (0:1–6:1). Viewed from top to bottom, Δδ values indicate binding of Ca^{2+} first in the C-terminal domain, followed by the N-terminal domain. Additionally, binding in one domain affects structural changes in the other. The gray arrows indicate direction of changes.

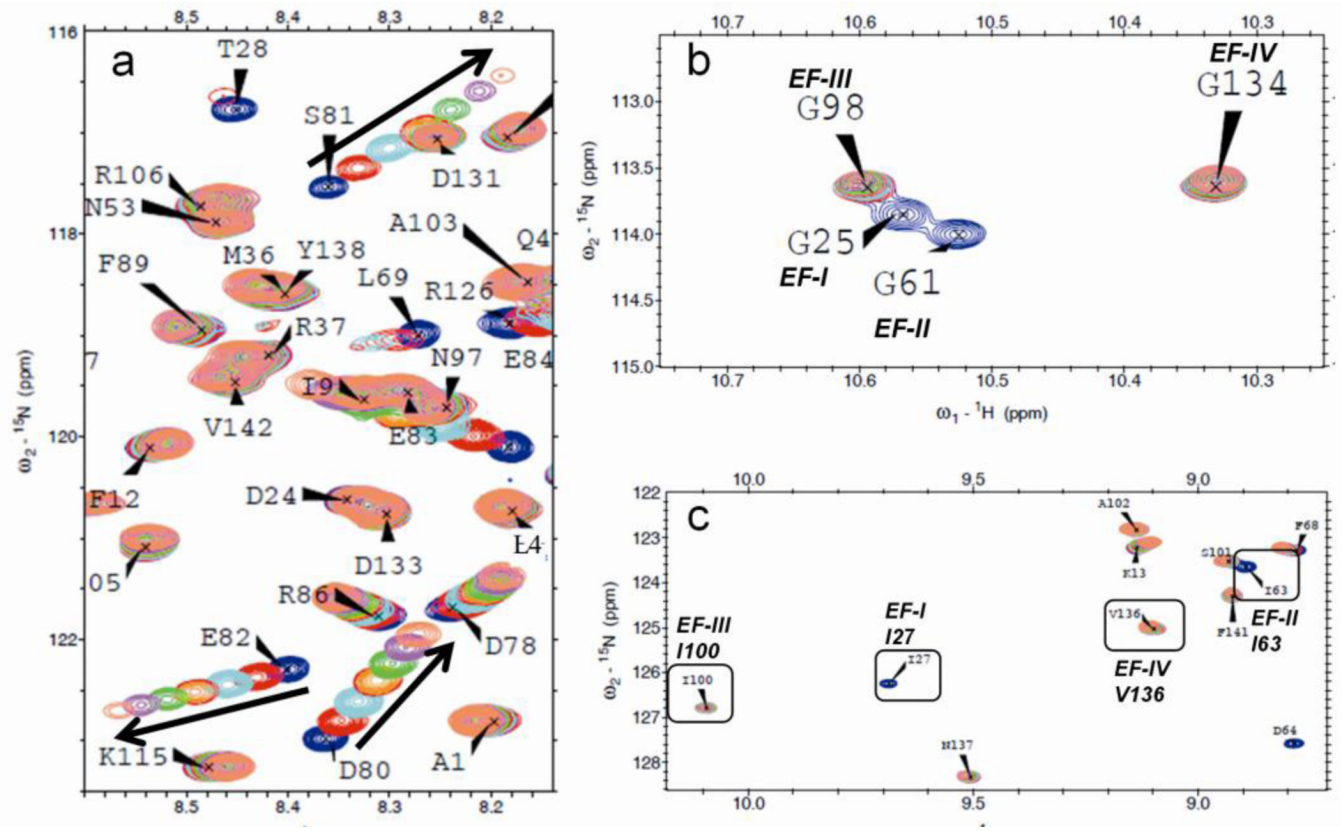

Fig. 5.

(**a**) Movement of HSQC peaks for CaM bound with 6 MEs Ca^{2+} followed by titration of Pb^{2+} from 0–3 MEs in 0.5 ME increments. Residues in the C-terminal domain exhibit stable chemical shifts, while significant changes are observed for residues D78, D80, S81, E82, E83 and R86, which suggests a potential Pb^{2+}-binding site in the linker region (74–82). (**b**) Residues in sites EF-I and EF-II, but not EF-III and EF-IV, disappear with addition of Pb^{2+} to Ca^{2+}:CaM complex. (**c**) Similar results are observed for residues I27 and I63 occupying position 8 in the EF loop regions of sites EF-I and EF-II only.

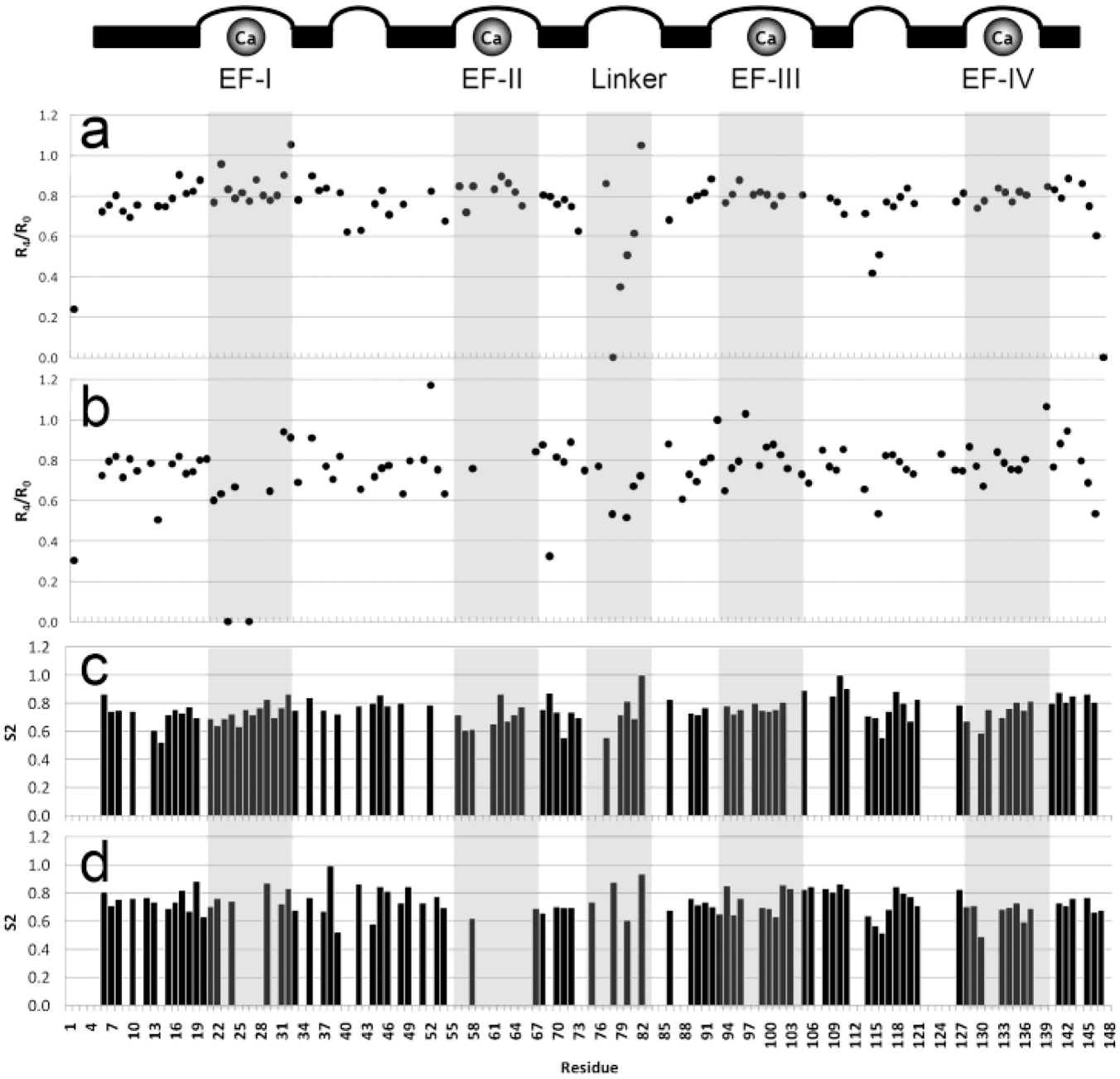

Fig. 6.

Comparison of NOE data for (**a**) Ca-CaM and (**b**) Ca-CaM with the addition of 2 MEs Pb^{2+}. Helices, loop regions and Ca^{2+}-binding sites are identified above the plots. Pb^{2+} appears to displace Ca^{2+} in the N-terminal domain but not the C-terminal domain, with additional binding in the linker region.

Table 1

Domain-specific binding dissociation constants for CaM.

	K_d (μM)	
Domain (Site)	**Ca(II)**	**Pb(II)**
[a]ND (I, II)	11.50±0.68	1.40±0.30
[b]CD (III, IV)	2.04±0.02	[c]0.73±0.10
CD (III, IV)	--	[d]0.67±0.06
CD (Secondary)	--	1.93±0.32

[a]N-terminal domain

[b]C-terminal domain

[c]Direct titration

[d]Competitive titration with Ca(II)